Numerical Simulation Study on the Effect of Combustion Parameters on Thermal Regenerative Ladle Baking

Lipeng WANG, Changxin LI, and Xuebo CHEN

Abstract—**The ladle is an indispensable container in the steel smelting process. Its baking efficacy directly affects the subsequent molten steel quality and smelting efficiency. In order to study the influence of the main control parameter air preheating temperature on the ladle baking process, this paper establishes a numerical model of the thermal regenerative ladle baking process, using ANSYS Fluent 2023R1 software and based on the standard k-ε turbulence model, the species transport model, and the DO radiation model. This paper analyzes the changing rules of temperature and NOx density distribution field in the ladle under different baking stages and air preheating temperatures. The results show that under the boundary conditions set by numerical simulation, the simulated temperature rise curves of baking are broadly in harmony with the standard temperature rise curves. Increasing the preheating temperature can effectively increase the combustion temperature, thus increasing the area of the high temperature zone and promoting energy saving. However, it also diminishes the uniformity of the temperature field and causes an exponential increase in NOx density. Therefore, the preheating temperature should be set reasonably to attain equilibrium among combustion efficiency, energy savings, and environmental performance.**

Index Terms—**Ladle baking, combustion fields, numerical simulation, energy saving, process parameter optimization**

I. Introduction

The ladle, as a container for carrying and transferring molten steel, has thermal states that directly affect the rate of temperature drop of the molten steel. It has an important influence on the overall temperature of the molten steel, and is one of the many factors that affect the temperature of the steel [1], [2]. To reduce the temperature loss during the steel transfer process and realize the objective of reducing the steel temperature out of the converter, it is necessary to Increase lining temperature as much as possible, thereby minimizing heat loss through the ladle [3]-[5]. The ladle saves molten steel at a temperature exceeding 1770 K throughout the steelmaking process. Despite the implementation of extensive insulation measures, the temperature disparity between the ladle's inside and outside remains substantial, and the heat loss on the lining and outlet layer surface cannot be neglected [6]. The heat loss of the ladle, as a commonly used piece of equipment, is significant. Consequently, the study of the ladle's thermal state, energy consumption, and NOx emission levels assumes paramount importance.

Compared to experimental studies, numerical modeling techniques show significant advantages in computational accuracy, simulation periods, and cost-effectiveness. Many scholars have studied the thermal state of the ladle by numerical simulation from different angles. For example, Khodabandeh et al.[7], [8] simulated the impacts of excess air and air temperatures on the on the heat-up efficiency of a burner within an industrial furnace. By comparing the numerical results with field measurements, the simulations were able to the gas flow and temperature distributions within the heater. Furthermore, the discrete-ordinate (DO) exhibited a superior performance counterpart to the P1 radiation model. Yuan et al.[9], [10] conducted a simulation study of a porous burner specifically designed for a heat storage ladle. They thoroughly analyzed the impact of different numbers of gas holes and injection angles on the temperature, velocity, and pressure. The results demonstrated that reducing the gas inlet diameter augments flame stiffness but concurrently diminishes the size of the high-temperature zone. Furthermore, the temperature field was found to be most uniform in the burner with an optimal injection angle of 20° and a nozzle configured with four holes.

Among other studies, Volkova et al. [11], [12] formulated a numerical heat transfer model based on Fourier differential equations to forecast the liner temperature field during ladle casting. The results show that the study reveals that preheating combustion air using flue gas, employing oxygen-enriched air, or changing the air ratio can significantly enhance the efficiency of ladle heating. This results in higher combustion temperature and lower flue gas volume. Tripathi et al. [13] developed a temperature model for predicting the temperature variations of ladle and molten steel and analyzed the temperature variations of ladle and molten steel. The results showed that slag thickness, discharge temperature, and ladle life have minimal effects, whereas the initial refractory temperature plays a crucial role. Krishnamurthy et al. [14], [15]conducted an evaluation and analysis of the flow and temperature field distributions in

Manuscript received September 24, 2024; revised March 6, 2025.

This work was supported by the National Natural Science Foundation of China, under grant numbers 71571091 and 71771112.

Lipeng Wang is a postgraduate student of School of Electronic and Information Engineering, University of Science and Technology Liaoning, Anshan 114051, China. (e-mail: 17662434145@163.com).

Changxin Li is a network engineer of School of Electronic and Information Engineering, University of Science and Technology Liaoning, Anshan 114051, China. (e-mail: 1367229898@qq.com).

Xuebo Chen is a professor of School of Electronic and Information Engineering, University of Science and Technology Liaoning, Anshan 114051, China. (corresponding author, e-mail: xuebochen@126.com).

combustion under air-fueled and oxygen-fueled conditions. The results of the study show that oxygen-enriched combustion exhibits enhanced energy utilization efficiency, along with uniform temperature and heat flux distributions. Caetano et al. [16] analyzed energy conversion and utilization of boiler combustion to recycle some of the thermal energy remaining in the boiler exhaust gas. The results show that the implementation of flue gas recirculation technology and heat regeneration technology provides a new method for energy saving and emission reduction, and provides a reference for practical process optimization.

The above scholars have thoroughly studied the ladle baking process from different perspectives. However, there are fewer studies on the whole baking process and its effect on NOx. In combustion, fuel and air are injected through a nozzle and ignited. For preheating air can accelerate the combustion reaction and significantly increase the combustion temperature, which is important for energy saving and emission reduction.

Combining field experience, the core of thermal storage baking is the heat reservoir, which will directly affect the enthalpy in the combustion reaction. This affects the combustion flame and flue gas temperature, which indirectly affects the baking efficiency of the ladle. Therefore, to optimize heat storage baking, it is necessary to evaluate the working parameters from the air preheating temperature's effect on the baking process. This is important for steel companies to save energy and reduce emissions.

This paper takes the regenerative ladle baker as the research object, and employs ANSYS Fluent 2023R1 software to conduct a numerical simulation of the ladle baking process. The research delves into the baking effects and NOx emissions during different baking stages and at different air temperatures. The main objective is to deepen the understanding of the baking process by numerically evaluating the combustion parameters, with the ultimate goal of optimizing the baking process and reducing production costs.

II. Numerical Modeling and Calculation Methods

A. Physical Modeling and Meshing

The thermal regenerative ladle possesses a high degree of symmetry. To reduce the computational complexity, the paper adopted a half-model for modeling. Figure 1 illustrates the model of the thermal regenerative ladle and its meshing. Specifically, Figure 1(a) displays a simplified schematic of the ladle, encompassing essential components like the ladle lid, burner, fluid domain, and lining. Among them, the burner is a concentric circular design. Detailed dimensions of the ladle and their representations are shown in Table 1. Based on the constructed physical model, hexahedral meshing was performed using ICEM-CFD software. Among other things, localised refinement of the burner is carried out. The generated mesh is shown in Fig. 1(b) and contains about 400,000 mesh elements.

TABLE 1
DIMENSIONAL MARKING OF THERMAL REGENERATIVE LADLES

Annotate	Hidden meaning	Value (mm)
H1	Combustion domain height	3720
H2	Overall height of ladle	4335
H3	Tundish lining thickness	310
H4	Flue gas outlet	115
D1	Inner diameter of the bottom of the ladle	2310
D2	Outer diameter of the bottom of the ladle	2910.5
D3	Inside diameter of the top of the ladle	2540
D4	Burner inner diameter	100
D5	Burner outer diameter	200
L	Spacing between burners	800

B. Basic Equations of the Model

The ladle baking process is a highly complex non-stationary combustion process in which the combustion and control systems are coupled with each other to form unique dynamic characteristics, accompanied by gas flow, heat transfer and radiation, and interactions between them. Therefore, the main controlling equations involved are the standard k-ε turbulence equation, the component transport

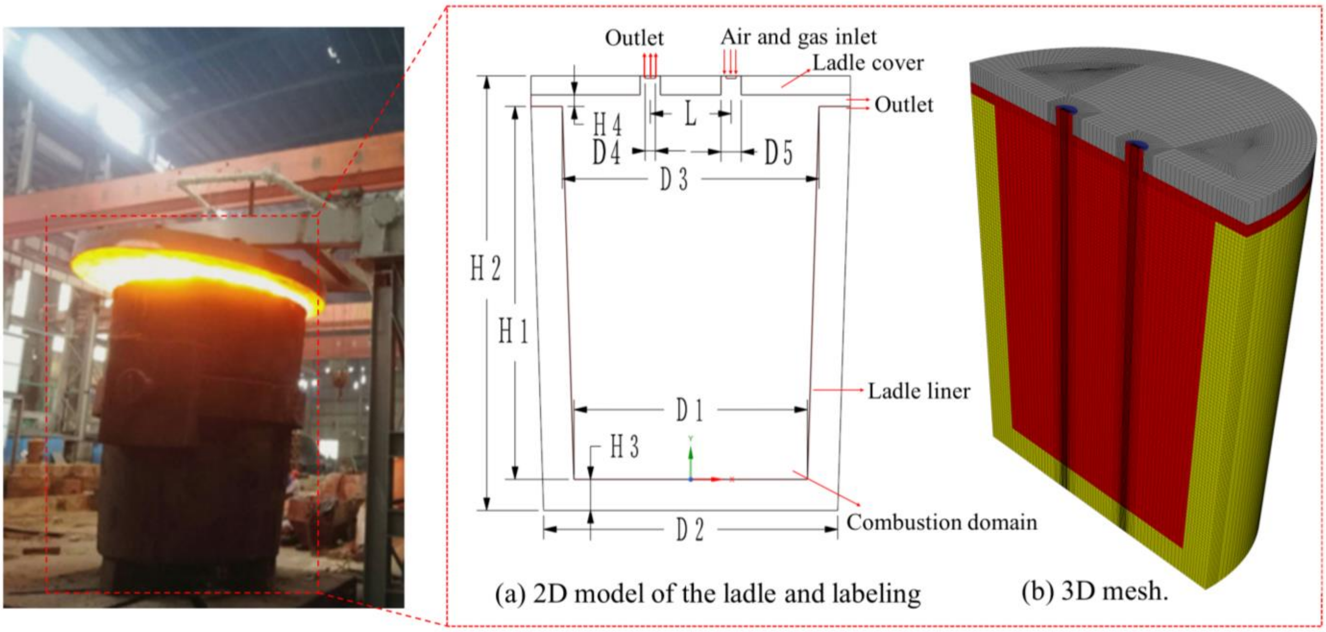

Fig. 1. Regenerative ladle baker model and its mesh.

equation, and the DO radiation equation, in addition to the three basic equations. The controlling equations are as follows. The control equations are as follows [17].

(1) Continuity equation

$$\frac{\partial \rho}{\partial t}+\frac{\partial(\rho u_i)}{\partial x_i}=0 \tag{1}$$

Where ρ is the density, kg/m^3; t is the time, s; u_i is the velocity components, m/s; x_i is the transmission distance, m.

(2) Energy equation

$$\frac{\partial \rho T}{\partial t}+\mathrm{div}(\rho\vec{u}T)=\mathrm{div}(\frac{k_1}{c_p}\mathrm{grad}T)+S_T \tag{2}$$

Where T is the temperature, K; $\vec{u}$ is the velocity vector; k_1 is the heat transfer coefficient; c_p is the specific heat capacity, J/(kg·K); S_T is the energy source term.

(3) The momentum equation

$$\frac{\partial}{\partial t}(\rho u_i)+\frac{\partial}{\partial x_j}(\rho u_i u_j)=-\frac{\partial p}{\partial x_j}+\frac{\partial \tau_{ij}}{\partial x_j}+\rho g_i+F_i \tag{3}$$

Where p is the pressure, Pa; τ_{ij} is the stress tensor; g_i and F_i are the volumetric force.

(4) The k-equation (6) and the ε-equation (7)

$$\frac{\partial \rho k}{\partial t}+\frac{\partial \rho k u_i}{\partial x_i}=\frac{\partial}{\partial x_j}[(\mu+\frac{\mu_t}{\sigma_k})\frac{\partial k}{\partial x_j}]+G_b +G_k-\rho\varepsilon-Y_M+S_k \tag{4}$$

$$\frac{\partial \rho \varepsilon}{\partial t}+\frac{\partial \rho \varepsilon u_i}{\partial x_i}=\frac{\partial}{\partial x_j}[(\mu+\frac{\mu_t}{\sigma_\varepsilon})\frac{\partial \varepsilon}{\partial x_j}]+ C_{\varepsilon 1}\frac{\varepsilon}{K}(\mathrm{G}_k+C_{\varepsilon 3}G_b)-C_{\varepsilon 2}\rho\frac{\varepsilon^2}{K}+S_\varepsilon \tag{5}$$

Where k is the turbulent kinetic energy, J; ε is the dissipation rate; u_i is the velocity component in the corresponding direction; x_i and x_j i is the transmission distance in the corresponding direction, m; μ is the effective kinetic viscosity, kg/(m·s); μ_t is the turbulent viscosity coefficient, kg/(m·s); G_k and G_b are the turbulent kinetic energy generated by the mean velocity gradient and induced by buoyancy, J, respectively; Y_M is the dissipation term due to turbulent pulsating expansion; S_k is the source term of k, kg/(m·s^3); S_ε is the source term of ε, kg(m·s^4); σ_k and σ_ε are the Prandtl numbers; In the standard k-ε model, σ_k =1.0, σ_ε=1.3, $C_{\varepsilon 1}$=1.44, $C_{\varepsilon 2}$=1.92, and $C_{\varepsilon 3}$=0.8.

(5) Component transport equation

$$\frac{\partial \rho c_s}{\partial t}+\mathrm{div}(\rho c_s)=\mathrm{div}[D_s\mathrm{grad}(\rho c_s)]+S_s \tag{6}$$

Where c_s is the mass fraction of component s; D_s is the diffusion coefficient of component s, m²/s; S_s represents the chemical reaction rate, mol /(L·s).

(6) Vortex dissipation model control equation

In the Eddy Dissipation model, the chemical reaction rate is controlled by turbulent mixing and is given by the smaller of the following two expressions:

$$R_{i,r}=(v''_{i,r}-v'_{i,r})M_{w,i}A\rho\frac{\varepsilon}{k}\min_R(\frac{Y_R}{v'_{R,r}M_{w,R}}) \tag{7}$$

$$R_{i,r}=(v''_{i,r}-v'_{i,r})M_{w,i}AB\rho\frac{\varepsilon}{k}\frac{\sum_P Y_P}{\sum_j^N v''_{j,r}M_{w,j}} \tag{8}$$

Where $R_{i,r}$ is the net production rate of component i due to reaction r, mol/s; $v_{i,r}''$ and $v_{i,r}'$ are the stoichiometric numbers of the product and reactant i in reaction r; Y_P and Y_R are the mass fractions of the product and reactant, respectively; A and B are empirical constants, A = 4 and B = 0.5; ε/k and is the large-vortex mixing time scale, which controls the rate of chemical reaction.

(7) DO (Discrete Ordinates) radiation model [18], [19]

$$\frac{dI(r,s)}{ds}+(\delta+\sigma_s)I(\vec{r},\vec{s})=\eta n^2\frac{\sigma T^4}{\pi}+ \frac{\sigma_s}{4\pi}\int_0^{4\pi}I(\vec{r},\vec{s}')\phi(\vec{s},\vec{s}')d\Omega' \tag{9}$$

Where η, σ_s and n are the absorption, scattering and refraction coefficients, respectively; I is the radiation intensity determined from $\vec{r}$ and $\vec{s}$, W/m^2; σ is a constant, σ=5.669×10^{-8}; ∅ for the phase function; Ω' for the steradian angle, sr.

Gas absorption coefficient determines the amount of radiation. The gas radiative emissivity is determined through the WSGGM model. The gas absorption coefficient and gas radiative emissivity are determined by Eqs. (12) and (13):

$$\eta=-\left(\frac{1}{L}\right)\ln(1-\delta) \tag{10}$$

$$\delta=\sum_{i=0}^{I}\eta_{\varepsilon,j}(T)\left(1-e^{-k_i pL}\right) \tag{11}$$

Where, L is the ray length, m; $\eta_{\varepsilon,j}$ is the absorption coefficient, m^{-1}.

C. Boundary Conditions and Solution Methods

In the research, the inlet uses the velocity inlet boundary condition; The gap between the cap and the ladle is the outlet, using pressure outlet, with the external ambient pressure;

the exhaust burner is set as a pressure outlet boundary condition with a level of -200 Pa; the excess air coefficient is 1.1; the ambient pressure is 101325 Pa; the acceleration of gravity is 9.8 m/s. Table 2 shows the refractory material and gas parameter settings.

TABLE 2
PHYSICAL PROPERTIES OF REFRACTORY MATERIALS AND GASES

Physical property	Coke oven gas	Refractory material
Thermal conductivity	volume-weighted -mixing-law	5.314-3.37×10^{-3} W·m^{-1}·K^{-1}
Specific heat	mixing-law	803+6.18×10^{-4} J·kg^{-1}·K^{-1}
Density	mass-weighted -mixing-law	2860 kg·m^{-3}

At the baking site, a baking stage can be divided into small, medium, and large fire stages. In this paper, the converter gas was used to simulate these three stages with gas flow rates of 0.11 m³/s, 0.17 m³/s, and 0.22 m³/s, respectively. The air preheating temperature is 1073 K, and the gas preheating temperature is 310 K. Table 3 outlines the composition of the converter gas. Table 4 shows the air and gas flow rates and velocities for the three baking stages of the ladle. At the same time, air temperatures of 273 K, 473 K, 673 K, 873 K, 1073 K, and 1273 K are used to investigate the effect of different air preheating temperatures on the baking process. The air and gas flow rates were fixed at 0.22 m³/s and 0.35 m³/s.

TABLE 3
THE MAIN COMPONENTS OF CONVERTER GAS (VOLUME CONCENTRATION)

CO	CO_2	H_2	N_2	O_2	H_2O
60.2%	14.6%	1%	18%	0.2%	5.7%

TABLE 4
RELEVANT SETTINGS FOR DIFFERENT BAKING STAGE CONDITIONS

Baking stage	Gas flow (m^3/s)	Air flow (m^3/s)	Gas flow rates (m/s)	Air velocity (m/s)
Small-fire	0.11	0.18	14.15	7.51
Medium-fire	0.17	0.27	21.23	11.27
High-fire	0.22	0.35	28.31	15.03

Solving method: In the model equation solving calculation, the solving algorithm adopts the SIMPLEC algorithm. The commutation time of the regenerative combustion is 60 S. Simulated baking time is 1800 S. In the transient calculation step, an adaptive time step is first used, and the fixed step size is then 0.125 S when the convergence curve stabilizes. This adjustment speeds up the computation without compromising accuracy.

III. MESH AND MODEL VALIDATION

A. Irrelevance Verification of the Mesh

The primary objective of the mesh-independence validation is to ascertain that the simulation results are independent of the number of meshes. This paper employed three mesh strategies for validation: coarse (200,000 cells), medium (400,000 cells), and fine (800,000 cells). The working conditions were set as follows: gas flow rate: 0.22 m^3/s; excess air coefficient: 1.1; baking time: 1800 S. Table 5 illustrates the average and maximum temperature results for the ladle combustion zone. Comparing the results, there is very little difference in the temperatures predicted by the three grid strategies. The overall temperature was about 5°C lower than the other two strategies when using a coarse grid of 200,000 cells; however, the difference was minimal when using medium and fine grids. In order to save computational time, a grid of 400,000 cells was chosen for subsequent calculations in this study.

TABLE 5
COMPARISON OF AVERAGE AND MAXIMUM TEMPERATURES IN THE COMBUSTION DOMAIN FOR THREE MESH DENSITIES

Degree of mesh density	Coarse	Medium	Fine
Average temperature (K)	1346.14	1349.9	1350.49
Maximum temperature (K)	2425.18	2421.4	2420.13

B. Model Validation

In this study, the aforementioned numerical model was performed and validated through the field monitoring data sourced from the literature [20]. The dimensional parameters of the ladle are as follows: the diameter of the bottom is 3240 mm, the diameter of the top is 3840 mm, and the height is 4060 mm. The layout of temperature monitoring points is shown in Figure 2, with the points positioned at distances of 100 mm, 700 mm, 1800 mm, and 3000 mm from the ladle's bottom. The constructed mathematical model was applied to the ladle structure and boundary conditions outlined in the literature. The simulation results and actual measurements are shown in Table 6. The results show that all errors are beneath 5%, falling within acceptable boundaries. The temperature at monitoring point 3 showed a large relative error, potentially attributable to either an actual flame displacement or inaccurate thermocouple monitoring. Consequently, the model presented in this paper is deemed suitable for simulation studies of the current ladle roaster.

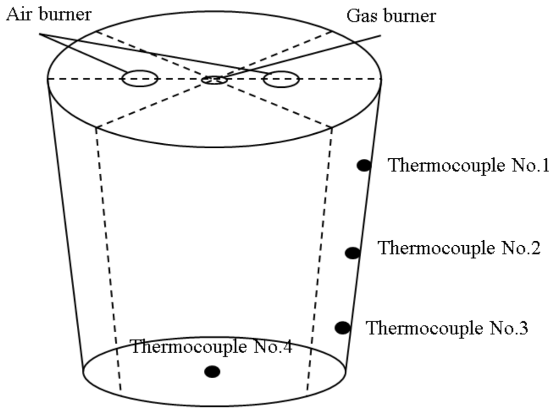

Fig. 2. Schematic diagram of thermocouple monitoring points inside the ladle in the literature.

TABLE 6
COMPARISON TABLE OF MEASURED AND ANALOGUE VALUES

Monitoring point	No.1	No.2	No.3	No.4
Measured value (K)	1383	1432	1485	1558
Analog value (K)	1348	1371	1406	1551
Relative error (%)	-2.5	-4.3	-5.3	0.44

IV. SIMULATION RESULTS AND ANALYSIS

A. Effect of Different Baking Stages on Ladle Flow and Temperature Fields

1) Impact on the flow field in the combustion domain

The flow state of gases within the ladle constitutes a pivotal factor influencing both temperature uniformity and heating rates, posing a notable research challenge during the baking process. Figure 3 describes the velocity streamlines for different cross sections under different baking stage conditions. Section heights are 100mm, 1700mm, and 3500mm.

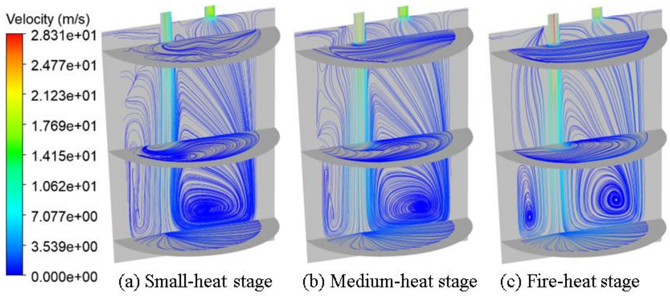

Fig. 3. Fluid velocity streamlines in the longitudinal section of the ladle at different baking stages.

In the figure, the gas and air injected into the left burner react with combustion to produce high-temperature flue gas. Upon reaching the ladle bottom, these flue gases disperse in all directions and subsequently ascend along the walls, and reflow into the bottom of the ladle, creating a vortex. The flue gas scrolling inside the ladle mainly occurs at the bottom, exhibiting a strong intensity at the bottom compared to the top, and on the left side compared to the right. As a result of the blower's extraction, the majority of combustion-generated flue gases are expelled through the right burner for thermal regenerative of the thermal regenerative body, preheating air for the next cycle. In conclusion, the regenerative ladle baker effectively diminishes flue gas emissions to the environment. The rotating airflow in the ladle prolongs the time that the flue gases are in the ladle, sustaining the continuous flame combustion. This, in turn, fosters a combustion environment conducive to high-temperature, low-oxygen combustion, thereby enhancing heat utilization efficiency and mitigating NOx emissions.

2) Effects on the temperature field distribution in the ladle

Figure 4 describes the longitudinal temperature distribution of the ladle under different baking stages. In the region of the left burner depicted, air and gas are injected and mixed for combustion, releasing substantial quantities of high-temperature flue gases. During the heat exchange process, these gases flow to the bottom of the ladle and the temperature progressively diminishes. After reaching the ladle bottom, the flue gases disseminate along the base towards the ladle wall. In the small fire baking stage shown in Figure 4(a), the gas flow rate is small, resulting in incomplete heat transfer from the gas, uneven temperature distribution, and high-temperature zones concentrated near the flame. When the baking stage reaches the medium fire stage illustrated in Figure 4(b), the degree of gas heat transfer is enhanced and uniformity is improved. When reaching the large fire stage illustrated in Figure 4(c), the flue gas temperature further increases, fulfilling the temperature specifications of the baking process. At this time, as gas flow increases, the flame thickens, and extends in length, and the high temperature area also expands correspondingly. In the combustion process, a region of lower temperatures appears at the outlet, which arises due to the induced draft fan causing the internal pressure of the ladle to be lower than the outside, thereby causing the ingress of outside air.

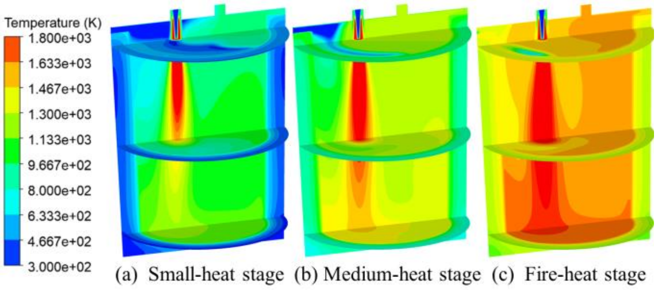

Fig. 4. Temperature field distribution under different baking stages.

Figure 5 describes the lateral temperature distribution at the heights of 100 mm, 1700 mm, and 3500 mm from the bottom at different baking stages. At a height of 100 mm, the temperature trends at each baking stage were consistent, showing an increasing and then decreasing trend. At a height of 1700 mm, the temperature showed a trend of rapid increase, slow decrease, and subsequent rapid increase. This external-high-internal-low temperature phenomenon is due to the rotating flow, which draws many high-temperature smoke suction furnace bottoms. When the distance from the bottom reaches 3500 mm, the temperature trend on the left side of the flame is similar to that at 1700 mm. At the flame, the temperature varies sharply, which is due to the incomplete combustion of a substantial quantity of low-temperature gas. On the left side of the flame, there is no clear pattern of temperature change due to the influx of air.

Figure 6 describes the ladle liner's actual and standard temperature rise curves. It is obvious from the figure that the temperature of the ladle lining increases steadily with the increase of baking time. The temperature difference between the two curves is very small, with a maximum of 31 K, which occurs at the medium temperature baking stage.

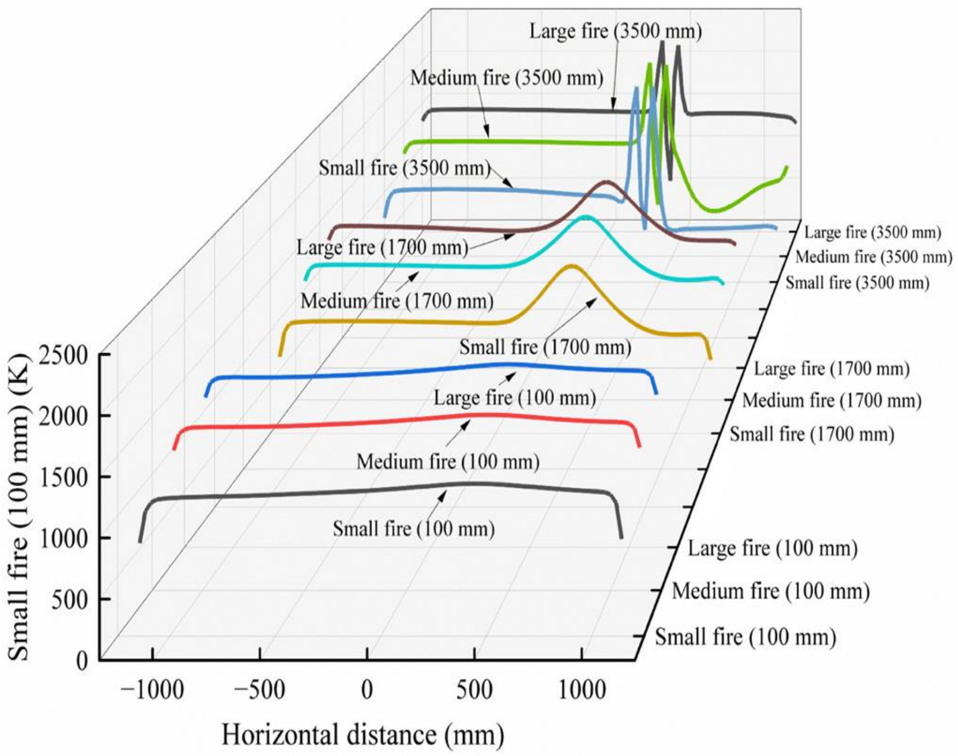

Fig. 5. Temperature distribution at different heights in the longitudinal section.

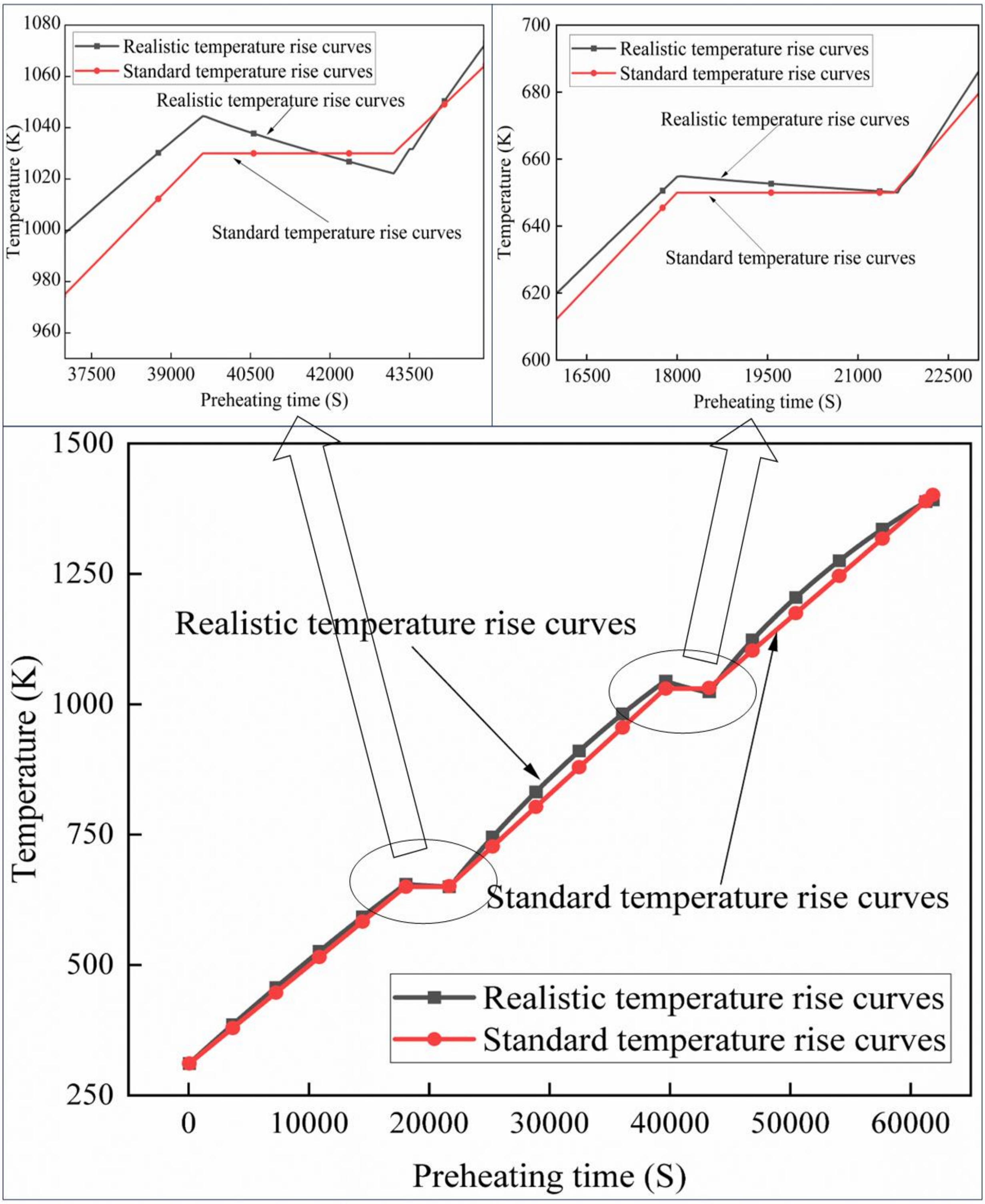

Fig. 6. Comparison results of average temperature of ladle lining and standard temperature rise figure.

During the preheat baking process, the warming curve of the low heat baking stage was more consistent with the standard warming curve. The temperature is higher in the medium and larger fire stages than the standard heating curve, but the heating speed gradually decreases. Considering that the physical properties of the ladle lining material are not constant, the existence of temperature difference is a normal phenomenon. At the end of each baking stage, the baking temperature is maintained within a small difference of 30 30 °C from the set temperature. The temperature dropped slightly by 5 K at the standstill moment of the low-fire stage and by 22 K at the standstill moment of the medium-fire stage. At the end of the high-temperature baking, the temperature of the ladle lining reaches 1391 K. which meets the requirements of the on-site baking temperature.

Effect of Different Air Preheating Temperatures on Ladle Temperature and NOx Density

3) Influence on the temperature field distribution in the ladle

Combined with field experience, the core component in a regenerative baking unit is the heat accumulator, It is used to preheat the air by recovering heat from the flue gas, which has an important influence on the gas combustion temperature.

Figure 7 delineates the combustion simulation results of the thermal storage ladle baker during the large-fire baking stage at preheating temperatures of 273 K-1273 K. It was observed that with the increase of air preheating temperature, the flame gradually became thicker, and the temperature of the whole temperature field showed a significant upward trend. In the transverse direction, the flue gas temperature shows a trend of low temperatures on both sides and high temperatures in the center. In addition, as the preheating temperature improves, the flame is capable of directly reaching the bottom of the ladle, resulting in a gradual expansion of the high-temperature zone above 1300 K. This result indicates that increasing the area covered by high temperature regions can be achieved by changing the remaining temperature of the air. The inclination of the flame tilt toward the right inner wall became increasingly pronounced during the flame jet. Consequently, when the air is preheated to higher temperatures, the flame length should be appropriately regulated to avoid the potential risk of high temperatures at the ladle's bottom.

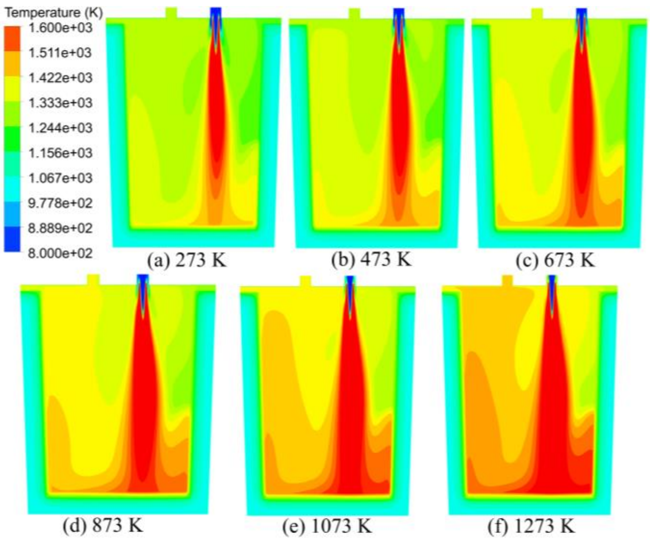

Fig. 7. Temperature cloud of ladle at different air preheating temperatures.

Figure 8 describes the effect of air preheating temperatures of 273 K-1273 K on the average and maximum temperatures within the combustion zone of the ladle. As the preheat temperature improves from 273 K to 1273 K, the average temperature in the combustion zone increases from 1291.2 K to 1408.2 K, and the maximum temperature increases from 2196.7 K to 2547 K. In addition, a distinct linear growth trend was observed in the average temperature within the combustion zone as the air preheating temperature increased. As the air preheating temperature increases, the maximum temperature shows an exponential increase and the average temperature shows a linear increase. For every 200 K improvement in the air preheating temperature, the average temperature improves by approximately 24.3 K.

Figure 9 describes the distribution of the circumferential mean temperature at different heights within the ladle, under different preheating temperature conditions. As can be seen from the figure, the average temperature decreases in a stepwise manner as the circumference height increases. Specifically, between 200 mm and 1500 mm, the temperature remains relatively stable. When the height reaches 1500 mm to 1800 mm, the temperature decreases sharply again, followed by a gradual deceleration in the temperature drop, leading to a stabilized temperature field. Above 3400 mm, close to the flue gas outlet, the temperature fluctuations increase again. When the preheating temperatures are set at 300 K, 473 K, 673 K, 873 K, 1073 K, and 1273 K, the temperature differences between the ladle's bottom and top are 133.42 K, 157.52 K, 187.86 K, 219.16 K, 251.36 K, and 284.17 K, respectively. The temperature difference increases linearly with increasing preheating temperature, indicating a decrease in uniformity.

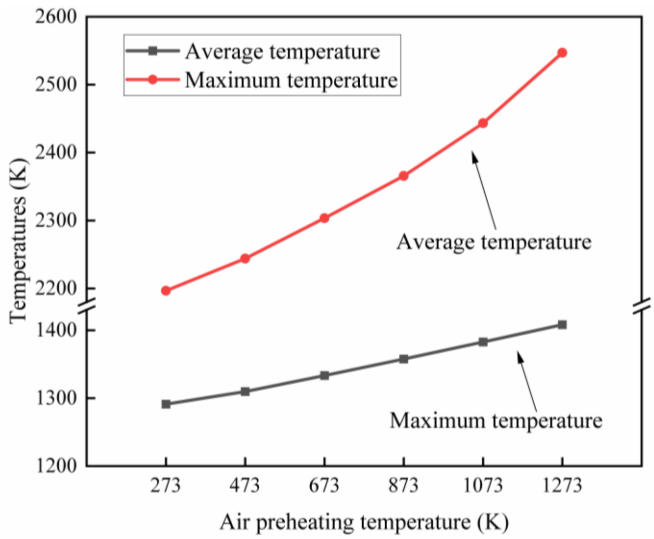

Fig. 8. Distribution of mean and maximum internal wall surface temperatures.

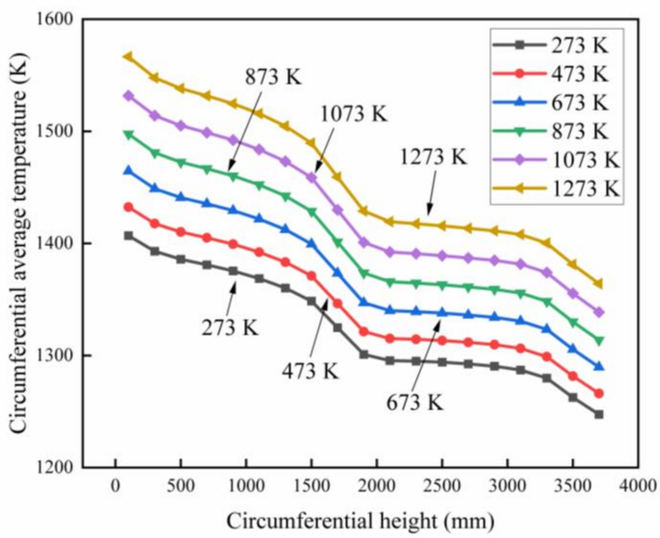

Fig. 9. Circumferential average temperature distribution at different heights of the ladle under different air preheating temperature conditions.

Figure 10 describes the plot of the longitudinal cross-sectional zone of the flame, delineated by the 1450 K isotherm as affected by the preheating temperature. When the preheating temperature was improved from 273 K to 1273 K, the longitudinal sectional area of the flame on the 1450 K isotherm increased exponentially from 1.33 m^2 to 6 m^2, with a gradual increase in the trend.

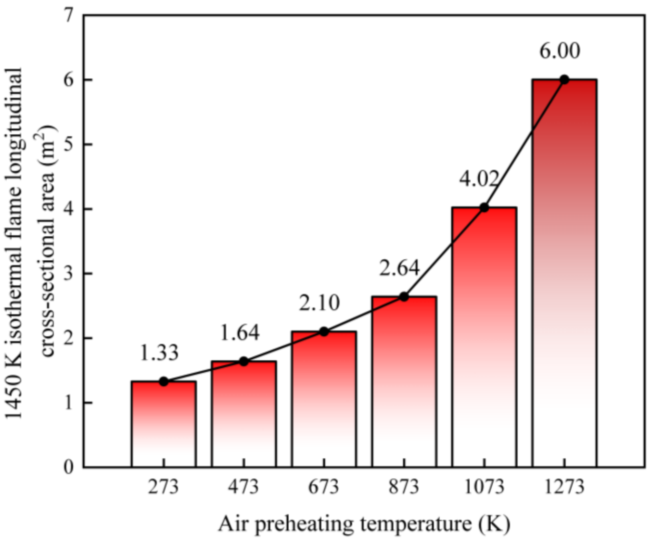

Fig. 10. Longitudinal cross-sectional area of 1450K isothermal flame at different air preheating temperatures.

4) Influence on the temperature distribution of the ladle lining

Figure 11 describes the temperature distribution of the ladle lining for air preheating temperatures of 273 K-1273 K, with a zoom in on the bottom area.

On the inner side of the ladle lining, the temperature progressively increases. Observing the enlarged area, the heating effect of the flame on the ladle lining becomes more pronounced as the preheating temperature improves, the heating effect of the flame on the ladle lining becomes more pronounced, resulting in a more expanded high-temperature zone and a more pronounced temperature increase at the ladle's bottom.

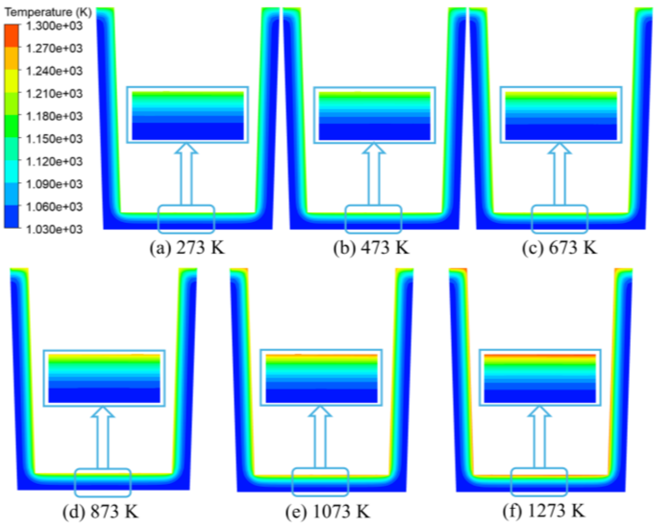

Fig. 11. Temperature distribution cloud of ladle lining under different air

Figure 12 describes the distribution of the impact of different air preheating temperatures on the baking process of the ladle lining. The results indicate that the baking temperature of the inner wall surface gradually increases as the preheating temperature improves. Notably, the baking temperature is substantially higher at the bottom of the ladle facing the burner, aligning with the temperature distribution observed at the combustion domain's edge.

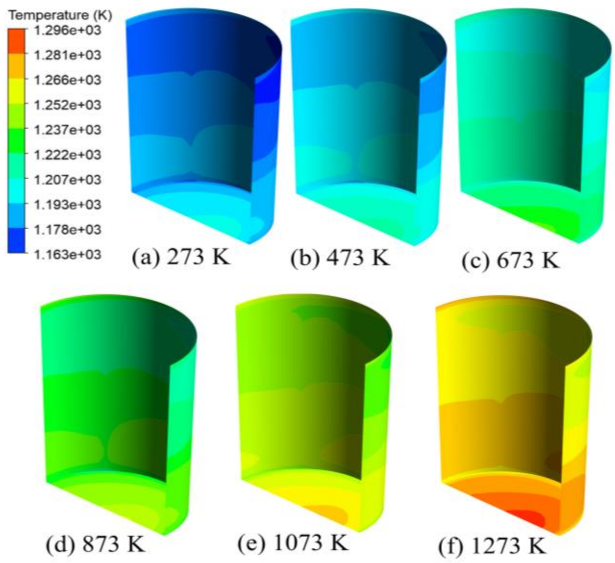

Fig. 12. Distribution of the effect of different air preheating temperatures on the baking of ladle liners.

Figure 13 describes the change in the temperature of the ladle lining for different preheating temperatures. The figure reveals a gradual increase in the ladle liner temperature over time, but the rate of increase decreases slightly. As the air preheating temperature increases, the heating time decreases, while the gas consumption per unit time remains consistent. When the air preheating temperatures are 473 K, 673 K, 873 K, 1073 K, and 1273 K, the respective reductions in the time required for the ladle lining to reach 1170 K are 8.3%, 17.5%, 25.8%, 32.5%, and 39.2%. The corresponding average temperatures at the end of the heating process are 1070.5 K, 1073.8 K, 1078.2 K, 1082.8 K, 1087.7 K, and 1092.8 K.

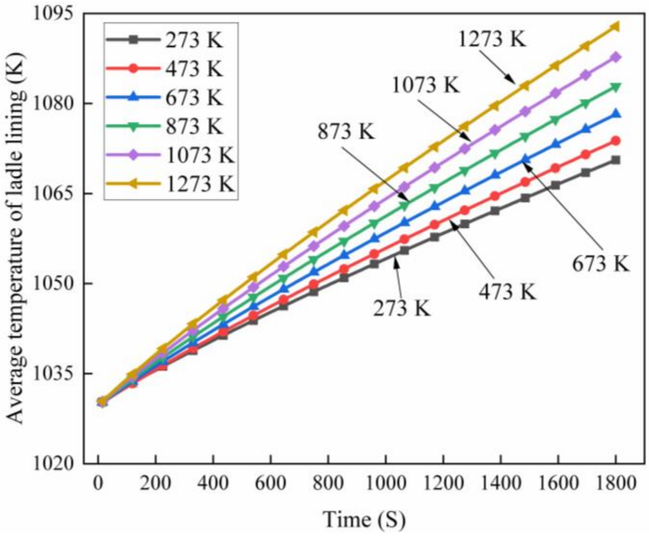

Fig. 13. The curve of average temperature of ladle lining as a function of time.

Figure 14 describes the distribution of average and maximum temperatures on the inner wall surface of the ladle for different air preheating temperatures. When the temperature is improved from 273 K to 1273 K, the average temperature of the wall surface increased linearly from 1180.5 K to 1268.2 K, and the maximum temperature increased from 1205.3 K to 1296.27 K, an increase of 87.6 K and 90.9 K, respectively. Analysis of the curve variations reveals that the inner wall surface temperature rises essentially linearly with an improvement in preheating temperature. Specifically, for each 200 K increment in temperature, the average temperature rises by approximately 17.5 K. In conclusion, improving the air preheating temperature during baking can increase the flame volume, thereby accelerating the heating rate, maximizing the baking temperature of the ladle liner, and ultimately facilitating energy conservation.

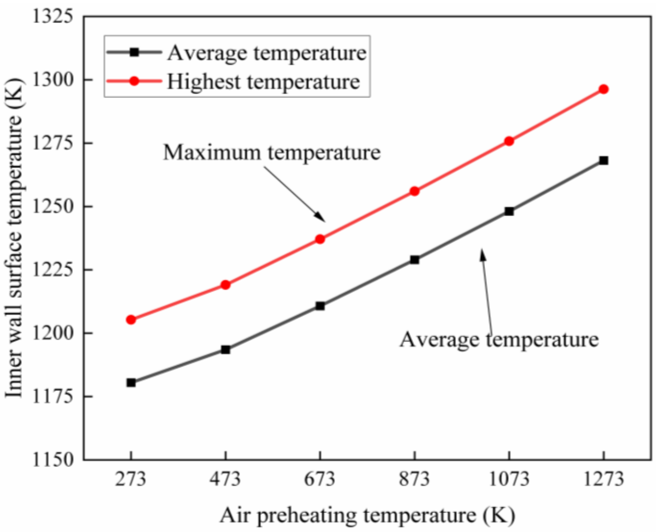

Fig. 14. Distribution of average and maximum temperatures on the inner wall surface of the ladle.

5) Impact on the distribution of NOx from combustion

During the combustion process, the NOx produced is mainly of the temperature type. Its production is influenced by the nitrogen and oxygen content, combustion temperature, and residence time in the high-temperature zone. Among these factors, temperature is the most significant influence on thermal NOx generation.

Figure 15 describes the temperature field at a temperature of 1073 K and the distribution of NOx density under different air preheating conditions. A comparison of Figure 7(a) with the NOx density distribution reveals a correlation between the NOx distribution and the temperature field. Specifically, the highest NOx density is found in the middle of the flame, and the NOx density increases gradually with rising temperatures. This is because NOx production requires the presence of nitrogen, oxygen, and high temperatures. At the initial stage of the reaction, despite the abundance of nitrogen and oxygen, the temperature is not hot enough for the chemical reaction to start. The NOx distribution is non-uniform due to the flow field, with higher concentrations in the flame center, the ladle bottom, and the near-wall regions. This distribution aligns with the temperature field, indicating that ambient temperature and the residence time of flue gases in the ladle significantly influence NOx production.

Figure 16 describes the trend of average NOx density at the outlet and within the combustion region. The preheating temperature significantly affects the variation of NOx density at both the outlet and the combustion region. The average NOx density at the outlet and in the combustion zone increases exponentially. This is attributed to the intensification of the reaction between nitrogen and oxygen at higher temperatures, which supplies sufficient energy for NOx formation, thus accelerating the generation rate and increasing its density. Notably, the NOx density in the combustion zone is significantly higher than at the outlet. This disparity is due to the use of regenerative combustion technology can effectively discharge most of the NOx through the burner and recycle it, thereby reducing emissions and environmental pollution.

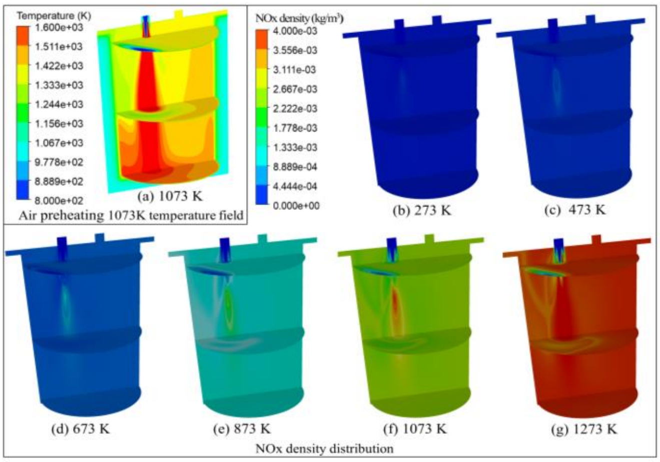

Fig. 15. Temperature field for air preheating at 1073 K and NOx density distribution for different preheating conditions.

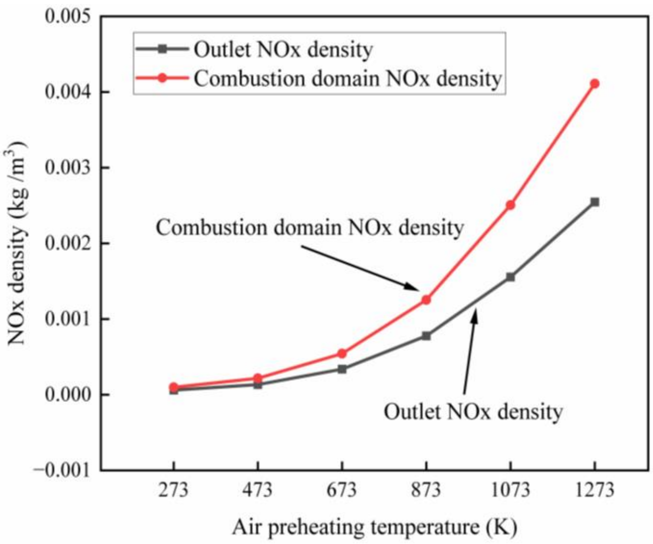

Fig. 16. Average Emission Curve of NOx Density at Steel Ladle Outlet and Combustion Domain.

V. Conclusion

In this paper, a multi-field coupled mathematical model for combustion, flow, and heat transfer during the baking process is developed using Fluent 2023R1 software, with the thermal regenerative ladle serving as the research object. The paper investigated the internal distribution characteristics of the ladle at different baking stages and air preheating temperatures. The studies provide a foundational basis for controlling the ladle's actual baking process and yield the following conclusions.

(1) Regenerative ladle baking minimizes flue gas emissions to the external environment, improves waste heat utilization, and minimizes NOx emissions. The dynamic flame allows for further enhancement of the flow action of

the flue gases and improves temperature uniformity and promotes heat transfer.

(2) Within the temperature field of the combustion domain, the temperature exhibits a stepwise decrement in the vertical direction, while the temperature differences the shows an increasing trend. Improve the air preheating temperature can significantly rise the flame volume during the thermal storage baking. When the temperature rises from 273 K to 1273 K, the longitudinal cross-sectional zone of the 1450 K isotherm of the flame expands from 1.33 m^2 to 6 m^2. Simultaneously, the temperature of the working layer of the ladle improved by approximately 22.3 K, with a saving coal gas of about 39.2%.

(3) During the process of combustion, the distribution of NOx has a strong correlation with temperature. The main areas of NOx production are located in the main combustion zone, while relatively small amounts of NOx are produced in areas of lower temperatures. The effect of combustion temperature on NOx shows a positive correlation.

(4) Through the simulation and analysis of the thermal regenerative ladle, it is possible to predict the rationality of the process parameters, thereby reducing research and development costs. In the future, our team will carry out research in terms of burner structure, which is of great theoretical and practical significance for energy saving and emission reduction.

References

[1] B. S. Chaikin, G. E. Maryanchik, E. M. Panov, P. T. Shaposhnikov, V. A. Vladimirov, I. S. Volovik, and B. A. Makarevich, "State. of. The. Art Plants for Drying and High-Temperature Heating of Ladles," Refractories and Industrial Ceramics, vol. 47, no.5, pp283-287, 2006

[2] Y. Liu, M. Ersson, and H. P. Liu, "A Review of Physical and Numerical Approaches for The Study of Gas Stirring in Ladle Metallurgy," Metallurgical and Materials Transactions B, vol. 50, pp555-577, 2019

[3] C. Gaber, M. Demuth, and R. Prieler, "An Experimental Study of a Thermochemical Regeneration Waste Heat Recovery Process Using a Reformer Unit," Energy, vol. 155, pp381-391, 2018

[4] S. E. Behery, A. A. Hussien, H. Kotbel, and M. E. Shafiel, "Performance Evaluation of Industrial Glass Furnace Regenerator," Energy, vol. 119, pp1119-1130, 2017

[5] F. Yuan, H. B. Wang, and P. L. Zhou, A. J. Xu, and D. F. He, "Heat Transfer Performances of Honeycomb Regenerators With Square or Hexagon Cell Opening," Applied Thermal Engineering, vol. 125, pp790-798, 2017

[6] B. Y. Lu, X. N. Meng, and M. Y. Zhu, "Numerical Analysis for The Heat Transfer Behavior of Steel Ladle as The Thermoelectric Waste-Heat Source," Catalysis Today, vol. 318, pp180-190. 2018

[7] E. Khodabandeh, M. Pourramezan, and M. H. Pakravan, "Effects of Excess Air and Preheating on The Flow Pattern and Efficiency of The Radiative Section of a Fired Heater," Applied Thermal Engineering, vol. 105, pp537-548, 2016

[8] Y. X. Su, and W. H. Wang, "Combustion Performance and NO Emission in Industrial Furnace Under Preheated Air Condition With Different Excess Air Ratio," Advanced Mterials Research, vol. 402, pp463 – 466, 2011

[9] F. Yuan, D. F. He, K. Feng, M. H. Zhang, and H. B. Wang, "Optimal Design and Experimental Study of Ejector for Ladle Baking," Steel Research International, vol. 89, no.12, 2018

[10] F. Yuan, H. B. Wang, P. L. Zhou, and A. J. Xu, "Combustion Performance of Nozzles With Multiple Gas Orifices in Large Ladles for Temperature Uniformity," Journal of Iron and Steel Research International, vol. 25, pp387-397, 2018

[11] O. Volkova, and D. Janke, "Modelling of Temperature Distribution in Refractory Ladle Lining for Steelmaking," ISIJ International, vol. 43, no.8, pp1185, 2003

[12] O. Volkova, "Ladle Heating Procedure and Its Influence on The Mgo–C-Oxidation, "Materials and Manufacturing Processes, vol. 23, no.8, pp758-763, 2008

[13] A. Tripathi, J. K. Saha, J. B. Singh, and S. K. Ajman, "Numerical Simulation of Heat Transfer Phenomenon in Steel Making Ladle," ISIJ International, vol.52, no.9, pp1591-1600, 2012

[14] N. Krishnamurthy, W. Blasiak, and A. Lugnet, "Development of High Temperature Air and Oxy-Fuel Combustion Technologies for Minimized CO2 and NOx Emissions in Industrial Heating," Proc. Joint Internat. Conf. on Sustainable Energy and Environment, pp1-3, 2004

[15] F. S. Qi, J. B. Shan, and B. K. Li, "Numerical Study on Ladle Baking Process of Oxy-Fuel Combustion," Thermal Science, vol. 24, no.6, pp3511-3520, 2020

[16] N. R. Caetano, B. P. Silva, A. C. Ruoso, A. G. Avila, L. A. O. Rocha, and G. Lorenzini, "Energy Recovery Based on Exhaust Gas Recirculation and Heat Regeneration Processes Applied in A Firewood Boiler," Journal of Engineering Thermophysics, vol. 32, no.3, pp482-501, 2023

[17] A. Khoshhal, M. Rahimi, and A. A. Alsairafi, "The CFD Modeling of NOx Emission, Hitac and Heat Transfer in an Industrial Boiler," Numerical Heat Transfer, Part A: Applications, vol. 58, no.4, pp295-312, 2010

[18] J. M. Loy, S. R. Mathur, and J. Y. Murthy, "A Coupled Ordinates Method for Convergence Acceleration of The Phonon Boltzmann Transport Equation," Journal of Heat Transfer, vol.137, no.1, 2015

[19] S. Park, J. A. Kim, C. Ryu, W. Yang, Y. J. Kim, and S. Seo, "Effects of Gas and Particle Emissions on Wall Radiative Heat Flux in Oxy-Fuel Combustion," Journal of Mechanical Science and Technology, vol. 26, pp1633-1641, 2012

[20] L. L. Ji, D. F. He, and A. J. Xu, "Numerical Simulation on Preheating System of Regenerative Ladle," Iron and Steel, vol. 48, no.4, pp76-81, 2013. (In China)